TECHNICAL ARTICLE

Temperature-dependent structure of an intermetallic ErPd₂Si₂ single crystal: a combined synchrotron and in-house X-ray diffraction study

Kaitong Sun [1,2,3,*] Yinghao Zhu,[1,3,*] Si Wu,[1,3,*] Junchao Xia,[1] Pengfei Zhou,[1] Qian Zhao,[1] Chongde Cao,[4,5,a)] and Hai-Feng Li[1,a)]

[1]*Joint Key Laboratory of the Ministry of Education, Institute of Applied Physics and Materials Engineering, University of Macau, Avenida da Universidade, Taipa, Macao SAR 999078, China*
[2]*State Key Laboratory of High Performance Ceramics and Superfine Microstructure, Shanghai Institute of Ceramics, Chinese Academy of Sciences, Shanghai 200050, China*
[3]*Guangdong-Hong Kong-Macao Joint Laboratory for Neutron Scattering Science and Technology, No. 1. Zhongziyuan Road, Dalang, Dongguan 523803, China*
[4]*Research and Development Institute of Northwestern Polytechnical University in Shenzhen, Shenzhen 518057, China*
[5]*School of Physical Science and Technology, Northwestern Polytechnical University, Xi'an 710072, China*

We have grown intermetallic ErPd₂Si₂ single crystals employing laser diodes with the floating-zone method. The temperature dependence of the unit-cell parameters was determined using synchrotron and in-house X-ray powder diffraction measurements from 20 to 500 K. The diffraction patterns fit well with the tetragonal *I4/mmm* space group (No. 139) with two chemical formulae within the unit cell. The synchrotron powder diffraction study shows that the refined unit-cell parameters are $a = 4.10320(2)$ Å, $c = 9.88393(5)$ Å at 298 K and $a = 4.11737(2)$ Å, $c = 9.88143(5)$ Å at 500 K, resulting in the unit-cell volume $V = 166.408(1)$ Å^3 (298 K) and $167.517(2)$ Å^3 (500 K). In the whole studied temperature range, no structural phase transition was observed. Upon cooling, the unit-cell parameters a and c are shortened and elongated, respectively. © *The Author(s), 2022. Published by Cambridge University Press on behalf of International Centre for Diffraction Data.* [doi:10.1017/S0885715622000100]

Key words: ErPd₂Si₂, structure, synchrotron and in-house X-ray powder diffraction, Rietveld refinement

I. INTRODUCTION

The ThCr₂Si₂-type structure is one of the most abundant structural prototypes of ternary intermetallics (Bażela *et al.*, 1997; Cao *et al.*, 2008; Frontzek, 2009; Shatruk, 2019), which shows a variety of interesting physical properties such as pressure-induced superconductivity in CePd₂Si₂ (Stewart, 2001), anomalous valence fluctuations in EuPd₂Si₂ (Stewart, 2001), and heavy fermion behavior (Shatruk, 2019). Among them, the erbium palladium silicide (ErPd₂Si₂) displays an anisotropic magnetic behavior along the three crystallographic axes at low temperatures (Sampathkumaran *et al.*, 2008). The ErPd₂Si₂ compound shows ferromagnetic ordering along the *c*-axis and antiferromagnetic ordering within the *ab* plane, according to the measurements of paramagnetic Curie–Weiss behavior derived from the high-temperature linear regime of the inverse magnetic susceptibility χ^{-1} (Sampathkumaran *et al.*, 2008). Furthermore, the magnetic susceptibility χ parallel to the *ab* plane shows a sharp peak at ∼3.8 K and a broad peak in the temperature range of 8–20 K. These were attributed to spin fluctuations with a finite antiferromagnetic component (Sampathkumaran *et al.*, 2008). Moreover, a neutron powder

diffraction study on polycrystalline ErPd₂Si₂ reveals a sine modulated magnetic structure (Bażela *et al.*, 1991). Later, polarized and unpolarized neutron diffraction studies reported two distinct antiferromagnetic modulations with respective propagation vectors at $Q_\pm = [H \pm 0.557(1), 0, L \pm 0.150(1)]$ and $Q_C = [H \pm 0.564(1), 0, L]$ for a ErPd₂Si₂ single crystal (Li *et al.*, 2015). The $Q_\pm$ modulation was attributed to localized 4*f* moments, whereas the Q_C was related to itinerant moments from conduction bands (Li *et al.*, 2015).

Intermetallic *RE*Pd₂Si₂ (*RE* = rare-earth) silicides (Sampathkumaran *et al.*, 1984; Stewart, 2001; Mazilu *et al.*, 2008; Frontzek, 2009; Xu *et al.*, 2011; Prokofiev, 2018) have the same tetragonal *I4/mmm* structure as the high-temperature structural phase of the family of 122-iron-pnictides (Sasmal *et al.*, 2008; Li *et al.*, 2009, 2010). There exist simultaneous antiferromagnetic and structural phase transitions for SrFe₂As₂ at ∼201.5 K upon cooling, from the high-temperature tetragonal phase (*I4/mmm*) to the low-temperature orthorhombic one (*Fmmm*). With hole or electron doping in the parent compound SrFe₂As₂, superconductivity appears with T_C up to 55 K after both the magnetic and structural phase transitions were suppressed (Rotter *et al.*, 2008; Sefat *et al.*, 2008; Torikachvili *et al.*, 2008).

Most of the previous studies on ErPd₂Si₂ were focused on the low-temperature regime (Yakinthos and Gamari-Seale, 1982; Bażela *et al.*, 1991, 1997; Tomala *et al.*, 1994; Szytuła *et al.*, 2001; Cao *et al.*, 2014; Uchima *et al.*, 2018),

---

and there exist few temperature-dependent studies, especially from the structural point of view. Therefore, we grew the intermetallic $ErPd_2Si_2$ single crystals and performed a temperature-dependent structural study up to 500 K. We carried out both in-house X-ray powder diffraction (XRPD) and synchrotron X-ray powder diffraction (SXRPD) measurements on a pulverized $ErPd_2Si_2$ single crystal to determine the temperature dependence of the unit-cell parameters and to check the potential structural phase transition.

II. EXPERIMENTAL

A. Single crystal growth

We prepared polycrystalline $ErPd_2Si_2$ samples with constituent metals of Er (99.98% purity), Pd (99.95% purity), and Si (99.99% purity) in a well-equipped arc-melting furnace (WK-11, Physcience Opto-electronics Co., Ltd.) under argon atmosphere (99.999% purity) at the University of Macau, Macao, China. Additional 3–5% mole Pd metal was added according to the stoichiometric ratio to supplement the loss due to volatilization. Having melted the mixture for three times, the ingot was ground manually, and the resulting powder was filled into plastic balloons for preparations of seed and feed rods. The balloon was shaped with a hydrostatic pressure of ~70 MPa. The prepared rods were sealed into cylindrical glass tubes with protecting argon gas and sintered at 950 °C for 36 h. After sintering, the samples are pure $ErPd_2Si_2$ phase without additional metals or impurity oxides. We grew the single crystals of $ErPd_2Si_2$ compound with the sintered rods treated additionally (Li *et al.*, 2021) by the floating-zone (FZ) technique using a well-equipped laser-diode FZ furnace (Model: LD-FZ-5-200W-VPO-PC-UM) at the University of Macau, Macao, China (Wu *et al.*, 2020). The growth conditions are similar to those reported previously (Cao *et al.*, 2014). It is stressed that the grinding and the shaping processes were carried out in a glove box. Scanning electron microscopy with energy-dispersive X-ray analysis of the grown $ErPd_2Si_2$ single crystal reveals a chemical stoichiometry of $Er_{1.00(5)}Pd_{2.10(7)}Si_{2.10(10)}$ (Figure 1), indicating ~5% vacancies on the Er site.

B. High-temperature synchrotron X-ray powder diffraction

An $ErPd_2Si_2$ single crystal was gently ground into powdered sample using a Vibratory Micro Mill (FRITSCH PULVERISETTE 0) with a vertical vibrating amplitude of 0.5 mm for 1.0 h for the SXRPD study. The grain size of the powdered sample is $4.07 \pm 0.97\,\mu m$ on average. The SXRPD measurements were performed on the beamline I11 at Diamond Light Source, Didcot, UK (Thompson *et al.*, 2009; Li *et al.*, 2014; Tang *et al.*, 2015). The beamline consists of an array of permanent magnets, three sets of slits, a double-crystal-monochromator composed of two liquid nitrogen cooled Si (111) crystals, a pair of double bounce harmonic rejection mirrors, and an intensity monitor comprising a thin Kapton scattering foil and a scintillation counter. The beamline comprises a transmission geometry X-ray instrument with a wide range of position-sensitive detectors. A triple-axis/two-circle diffractometer with high precision rotary stages was used. Synchrotron X-rays with a wavelength of
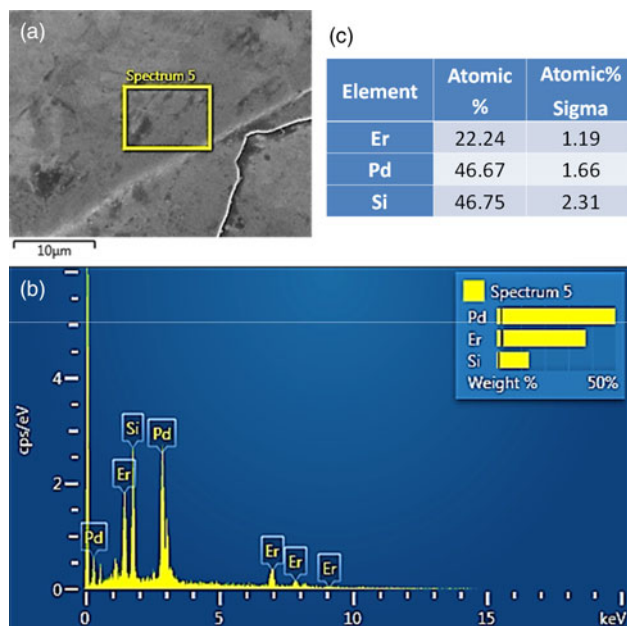

Figure 1. (a) Scanning electron microscopy image of the $ErPd_2Si_2$ single crystal with a scale bar of $10\,\mu m$. (b) Energy-dispersive X-ray analysis of the $ErPd_2Si_2$ single crystal. (c) Atomic ratio of Er, Pd, and Si elements in the $ErPd_2Si_2$ single crystal.

$\lambda = 0.827032$ Å were chosen as the radiation source. High-resolution SXRPD patterns were collected over a diffraction 2θ angle range of 9–66° at 298 and 500 K. The 2θ step interval is 0.001°, and the counting time is 1800 s (for 298 and 500 K) and 3600 s (for 500 K). The $ErPd_2Si_2$ powder was loaded onto the external surface of a 0.3-mm diameter borosilicate glass capillary tube by applying a thin layer of hand cream to it. The capillary sample holder was mounted directly on a magnetic spinner and in the center of the θ circle faceplate. The magnetic spinner keeps rotating around the vertical axis of the sample holder plate during the SXRPD measurements. The rotation technique is effective to obtain quality diffraction profiles and to minimize absorption and preferred orientation. The sample temperature was controlled using the beamline hot air blower and detected by a thermocouple near the sample. The symmetric θ-2θ scan technique was used for data collection (Thompson *et al.*, 2009; Tang *et al.*, 2015).

C. Low-temperature in-house X-ray powder diffraction

The same powdered $ErPd_2Si_2$ sample was used for an in-house X-ray powder diffraction study. The measurements were carried out on a Rigaku, SmartLab 9 kW X-ray diffractometer employing Cu $K_{\alpha 1} = 1.54056$ Å radiation and a 2D multidimensional semiconductor detector. XRPD patterns were collected at a voltage of 45 kV and a current of 200 mA. The 2θ range was from 30 to 78° with a step size of 0.005°. The measurements were performed at 20, 100, and 200 K with a dwell time of 1.0 h at each temperature.

D. Rietveld refinements

The computer program FULLPROF SUITE (Rodríguez-Carvajal, 1993) was used to analyze all powder

diffraction data. The initial crystal structure model was obtained from a room-temperature XRPD study (Li *et al.*, 2015). The peak profile shape was modeled with a Pseudo-Voigt function. The background was refined using linear interpolation between automatically identified background points. We considered the parameters relevant to improving refinement results, including scale factor, zero shift, peak shape parameters, asymmetry, preferred orientation, unit-cell parameters, atomic positions, as well as isotropic thermal parameter B. The refining procedure is as follows: (i) First, we refined the scale factor, zero shift, and unit-cell parameters. (ii) Second, we refined the peak shape parameters and background points. (iii) Third, we refined the atomic positions, thermal parameters, asymmetry, and preferred orientation step by step. Furthermore, we tentatively refined the strain effect on the collected data with a general strain broadening model (quartic form).

III. RESULTS AND DISCUSSION

A. High-temperature structure from the SXRPD study

Compared to in-house X-ray powder diffraction and neutron powder diffraction data, SXRPD holds the highest resolution for studying structural phase transitions by detecting possible Bragg peak splitting and observing appearance of additional Bragg peaks. Figure 2 displays the SXRPD patterns of ErPd$_2$Si$_2$ measured at 298 K for 0.5 h [Figure 2(a)] and 500 K for 0.5 h [Figure 2(b)] and for 1.0 h [Figure 2(c)]. All observed patterns were refined satisfactorily in the tetragonal $I4/mmm$ model. All the Bragg peaks recorded were accounted for (insets of Figure 2). Table I lists values of the refinement reliability parameters, R_p, R_{wp}, and R_{exp}, as well as the goodness of fit χ^2. These values are acceptable within the present experimental accuracy, which validates the FULLPROF refinements. By carefully checking the patterns at 298 K [Figure 2(a)] and 500 K [Figures 2(b) and 2(c)], we confirm that there is no structural phase transition as temperature increases from 298 to 500 K.

The unit cell of the refined structural model is shown in Figure 3, where Er, Pd, and Si ions were marked. It is noticed that the Pd and Si layers are staggered with a separation of the Er layer. Among the atomic positions of Er, Pd, and Si, only the z coordinate of Si ions may change. The electric and magnetic properties of ErPd$_2$Si$_2$ compound, e.g., anisotropic magnetoresistance, are determined by the Er ions and their coupling between interlayers, as well as the position of Si ions.

Since the splitting degree of Bragg peaks will become larger and larger as the diffraction angle increases, the diffraction data at higher 2θ angles is better used to monitor possible structural phase transitions. Figure 4 shows the SXRPD patterns as well as the corresponding FULLPROF refinements in the 2θ range of 50.3–54.8°. The Bragg peaks are indexed as (4 1 3), (3 3 2), (4 0 4), (2 1 9), (2 2 8), (1 1 10), and (4 2 0) as marked in Figure 4(b). The refinements for 298 and 500 K data show no splitting of the (4 1 3), (3 3 2), and (4 0 4) Bragg peaks.

SXRPD patterns collected at 500 K for 0.5 h [Figure 2(b)] and for 1.0 h [Figure 2(c)] were collected to check the effect of counting time on Rietveld refinements. As listed in Table I, the reliability values of R_p, R_{wp}, and R_{exp} for the data collected at 500 K with counting time of 0.5 h are higher than those of the
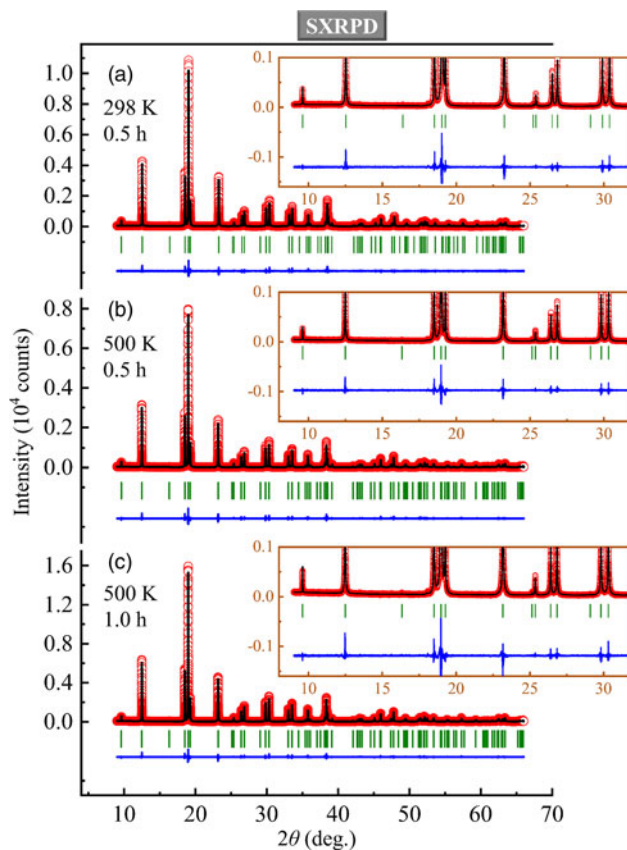

Figure 2. Observed (circles) and calculated (solid lines) synchrotron X-ray powder diffraction patterns of a pulverized ErPd$_2$Si$_2$ single crystal, collected at (a) 298 K, 0.5 h; (b) 500 K, 0.5 h; and (c) 500 K, 1.0 h. Vertical bars mark the positions of Bragg reflections. The bottom curves represent the difference between observed and calculated patterns. The diffraction angle 2θ is in the range of 9–66°. Insets of (a), (b), and (c) display their respective enlarged patterns in the 2θ range of 8–32°.

TABLE I. Experimental conditions and refinement parameters for the SXRPD study of single-crystal ErPd$_2$Si$_2$ compound.

T (K)	298	500	500
Counting time (h)	0.5	0.5	1.0
R_p	7.79	8.95	7.44
R_{wp}	10.20	11.70	9.43
R_{exp}	7.70	9.12	6.48
χ^2	1.74	1.64	2.12
R_p (strain)	7.54	8.67	6.99
R_{wp} (strain)	9.92	11.50	8.97
R_{exp} (strain)	7.73	9.13	6.51
χ^2 (strain)	1.65	1.59	1.90

data with counting time of 1.0 h, indicating that a higher counting time increases the ratio of intensity/background. Whereas the goodness of fit ($\chi^2 = 1.64$) of 0.5 h data is smaller than that (2.12) of the 1.0 h data, which we attribute to the enhancement of diffracted intensity. Finally, the data with a longer counting time also does not show Bragg-peak splitting and newly-appeared Bragg peaks.

The refined structural parameters of all patterns are included in Table II. The unit-cell parameter a of ErPd$_2$Si$_2$ is 4.10320(2) Å at 298 K and 4.11737(2) Å at 500 K, displaying an increase with temperature. The unit-cell parameter c is
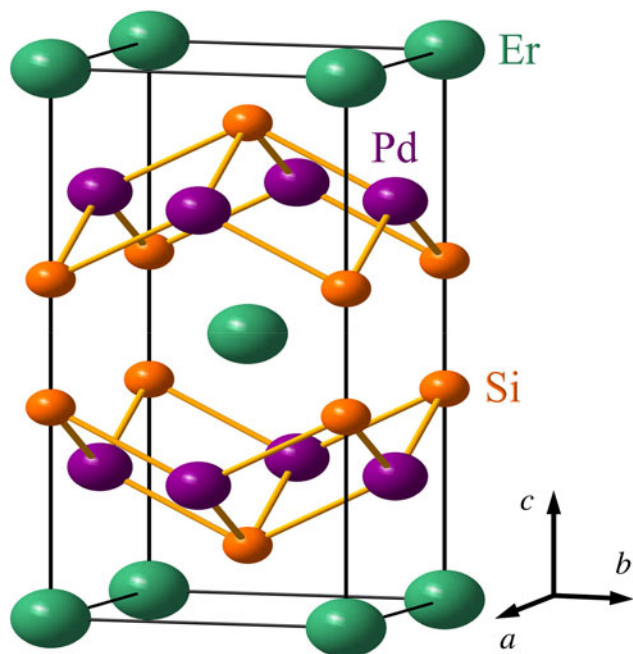
Figure 3. View of the unit cell of ErPd$_2$Si$_2$ in space group *I4/mmm* (No. 139). The Er, Pd, and Si ions are labeled.
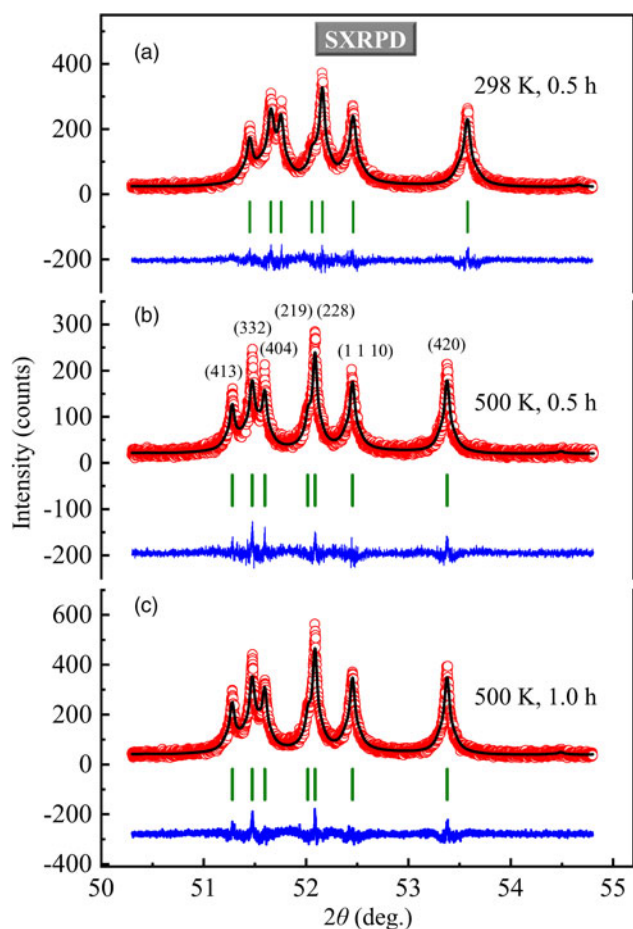

Figure 4. Observed (circles) and calculated (solid lines) synchrotron X-ray powder diffraction patterns of a pulverized ErPd$_2$Si$_2$ single crystal in the 2θ range of 50.3–54.8°. The patterns were collected at (a) 298 K, 0.5 h; (b) 500 K, 0.5 h; and (c) 500 K, 1.0 h. Vertical bars mark the positions of bragg reflections. The bottom curves represent the difference between observed and calculated patterns. The Bragg peaks of (4 1 3), (3 3 2), (4 0 4), (2 1 9), (2 2 8), (1 1 10), and (4 2 0) were marked.

TABLE II. Refined structural parameters of an intermetallic ErPd$_2$Si$_2$ single crystal from the SXRPD study, obtained from FULLPROF refinements of the SXRPD data collected on the I11 beamline (Diamond, UK) at 298 and 500 K.

SXRPD study of a pulverized ErPd$_2$Si$_2$ single crystal

(Tetragonal, space group: *I4/mmm*)

T (K)	298	500
Counting time (h)	0.5	0.5
a (Å)	4.10320(2)	4.11737(2)
c (Å)	9.88393(5)	9.88143(5)
V (Å^3)	166.408(1)	167.517(2)
D_{cal} (g cm^{-3})	8.706	8.649
Er	2a: (0, 0, 0)	
B (Er) (Å^2)	0.823(11)	1.183(7)
Pd	4d: (0, 0.5, 0.25)	
B (Pd) (Å^2)	0.860(11)	1.256(9)
Si	4e: (0, 0, z)	
z (Si)	0.38064(14)	0.37984(13)
B (Si) (Å^2)	1.200(27)	1.226(25)

The Wyckoff sites of all atoms are listed.

equal to 9.88393(5) Å at 298 K and 9.88143(5) Å at 500 K, showing a decrease upon warming. The unit-cell volume V = 166.408(1) Å^3 at 298 K and 167.517(2) Å^3 at 500 K, expanded by ~0.67% with temperature. This is accompanied by a decrease in density from 8.706 g cm^{-3} (298 K) to 8.649 g cm^{-3} (500 K). The refined results show a lattice shrinkage along the *c*-axis and an extension along the *a*-axis upon warming. The tetragonal crystal system does not change in the studied temperature range. The detailed synchrotron X-ray powder diffraction data at 298 K was indexed in Table III.

In the ThCr$_2$Si$_2$-type structure (Figure 3), Er ions are located at the Wyckoff site 2a (0, 0, 0), and Pd ions are fixed at 4d (0, 0.5, 0.25). The Si ions stay at 4e (0, 0, z) with only one degree of freedom along the coordination *z*-axis. The *z*-coordinates of Si ions were refined to 0.38064 (14) at 298 K and 0.37984(13) at 500 K.

B. Low-temperature structure from the in-house XRPD study

Figure 5 shows the XRPD diffraction patterns collected at 20 K [Figure 5(a)], 100 K [Figure 5(b)], and 200 K [Figure 5 (c)], as well as the corresponding structural refinements. We meticulously examined the temperature evolution of the shape and position of Bragg peaks. Overall, the collected data can be effectively indexed with the *I4/mmm* space group. The extracted crystallographic information, such as unit-cell parameters and atomic positions as well as the goodness of fit, is listed in Table IV. The unit-cell parameters a and c increase by ~0.17% and decrease by ~0.11%, respectively, as the temperature rises from 20 to 200 K. Temperature variances in unit-cell parameters cause an expansion of the unit-cell volume and a decrease of the calculated density by ~0.23% with temperature.

C. Strain effect

Although the values of goodness of fit are low enough for a good FULLRPOF refinement, for example, $\chi^2 = 1.74$ for the refinement of SXRPD data collected at 298 K (Table I), and $\chi^2 = 1.43$ for the refinement of XRPD data collected at 100 K

TABLE III. Powder diffraction data of ErPd$_2$Si$_2$ from the SXRPD study with $\lambda = 0.827032$ Å at 298 K.

$2\theta_{obs}$ (°)	d_{obs} (Å)	$(I/I_0)_{obs}$	h	k	l	$2\theta_{cal}$ (°)	d_{cal} (Å)	$\Delta 2\theta$ (°)
9.596	4.9440	2.03	0	0	2	9.600	4.9420	−0.0044
12.525	3.7908	29.51	1	0	1	12.529	3.7896	−0.0041
18.522	2.5695	30.59	1	0	3	18.526	2.5690	−0.0043
19.022	2.5026	100.00	1	1	2	19.026	2.5021	−0.0042
19.263	2.4715	15.94	0	0	4	19.267	2.4710	−0.0036
23.252	2.0520	34.80	2	0	0	23.256	2.0516	−0.0039
25.207	1.8951	0.44	2	0	2	25.211	1.8948	−0.0041
25.392	1.8815	2.73	1	1	4	25.396	1.8812	−0.0038
26.496	1.8044	8.53	2	1	1	26.500	1.8042	−0.0042
26.849	1.7812	11.57	1	0	5	26.853	1.7809	−0.0042
29.892	1.6033	15.09	2	1	3	29.896	1.6031	−0.0038
30.371	1.5787	19.34	2	0	4	30.375	1.5785	−0.0044
33.119	1.4509	11.97	2	2	0	33.123	1.4507	−0.0039
33.552	1.4327	17.07	1	1	6	33.556	1.4325	−0.0044
35.539	1.3550	1.70	3	0	1	35.543	1.3548	−0.0045
35.810	1.3450	10.58	2	1	5	35.814	1.3449	−0.0038
36.080	1.3353	1.96	1	0	7	36.084	1.3351	−0.0039
38.213	1.2633	3.40	3	0	3	38.217	1.2632	−0.0045
38.472	1.2551	23.56	3	1	2	38.476	1.2550	−0.0041
38.599	1.2512	8.57	2	2	4	38.603	1.2510	−0.0039
39.104	1.2356	3.29	0	0	8	39.108	1.2355	−0.0037
42.191	1.1489	0.88	3	1	4	42.195	1.1488	−0.0038
42.905	1.1307	1.91	3	2	1	42.909	1.1306	−0.0038
43.137	1.1249	2.65	3	0	5	43.141	1.1248	−0.0036
43.369	1.1191	2.35	2	1	7	43.373	1.1190	−0.0043
45.213	1.0758	3.91	3	2	3	45.217	1.0757	−0.0043
45.879	1.0610	0.72	1	0	9	45.883	1.0609	−0.0044
45.992	1.0585	7.86	2	0	8	45.996	1.0584	−0.0037
47.542	1.0259	3.32	4	0	0	47.546	1.0258	−0.0038
47.864	1.0194	10.25	3	1	6	47.868	1.0193	−0.0045
49.365	0.9902	1.21	4	1	1	49.369	0.9902	−0.0038
49.574	0.9863	3.25	3	2	5	49.578	0.9863	−0.0043
49.782	0.9825	0.70	3	0	7	49.786	0.9824	−0.0045
51.448	0.9527	2.47	4	1	3	51.452	0.9527	−0.0045
51.653	0.9492	4.07	3	3	2	51.657	0.9491	−0.0040
51.754	0.9475	2.98	4	0	4	51.758	0.9474	−0.0040
52.053	0.9424	0.92	2	1	9	52.057	0.9423	−0.0042
52.156	0.9407	5.04	2	2	8	52.160	0.9406	−0.0036
52.457	0.9357	4.04	1	1	10	52.461	0.9356	−0.0042
53.573	0.9176	4.43	4	2	0	53.577	0.9175	−0.0042
54.661	0.9007	0.15	3	3	4	54.665	0.9006	−0.0042
55.443	0.8889	2.06	4	1	5	55.447	0.8889	−0.0038
55.635	0.8861	0.98	3	2	7	55.639	0.8861	−0.0036
56.209	0.8778	0.72	1	0	11	56.213	0.8777	−0.0037
57.467	0.8602	4.09	4	2	4	57.471	0.8601	−0.0045
57.745	0.8564	0.33	3	0	9	57.749	0.8563	−0.0039
59.442	0.8341	2.22	3	3	6	59.446	0.8340	−0.0037
60.267	0.8237	0.43	0	0	12	60.271	0.8237	−0.0041
60.742	0.8179	0.59	4	3	1M	60.746	0.8178	−0.0039
61.105	0.8135	0.72	4	1	7	61.109	0.8134	−0.0043
61.646	0.8070	1.08	2	1	11	61.650	0.8070	−0.0037
62.565	0.7964	1.19	4	3	3M	62.569	0.7963	−0.0036
62.747	0.7943	3.92	5	1	2	62.751	0.7942	−0.0044
63.100	0.7903	0.47	3	2	9	63.104	0.7903	−0.0043
63.191	0.7893	2.37	4	0	8	63.195	0.7892	−0.0037
63.457	0.7863	4.17	3	1	10	63.461	0.7863	−0.0037
65.423	0.7652	0.13	5	1	4	65.427	0.7652	−0.0043
65.499	0.7644	1.28	2	0	12	65.503	0.7644	−0.0042
65.953	0.7597	0.34	5	2	1	65.957	0.7597	−0.0044

$\Delta 2\theta$ (°) = $2\theta_{obs}$ (°) − $2\theta_{cal}$ (°). The Smith-Snyder figure-of-merit F_{20} = 195.12 (0.0041, 25) (Smith and Snyder, 1979), and the de Wolff figure-of-merit M20 = 134.37 (de Wolff, 1968). The peaks that contain intensity contributions from multiple reflections are labeled with "M".

(Table IV), we still tried to refine the strain parameters with an introduction of a general strain broadening model (quartic form) for the collected data. As listed in Table I, the values of reliability parameters and goodness of fit get a little smaller with refinements including the strain parameters, indicating small strains exist in the pulverized powder sample.
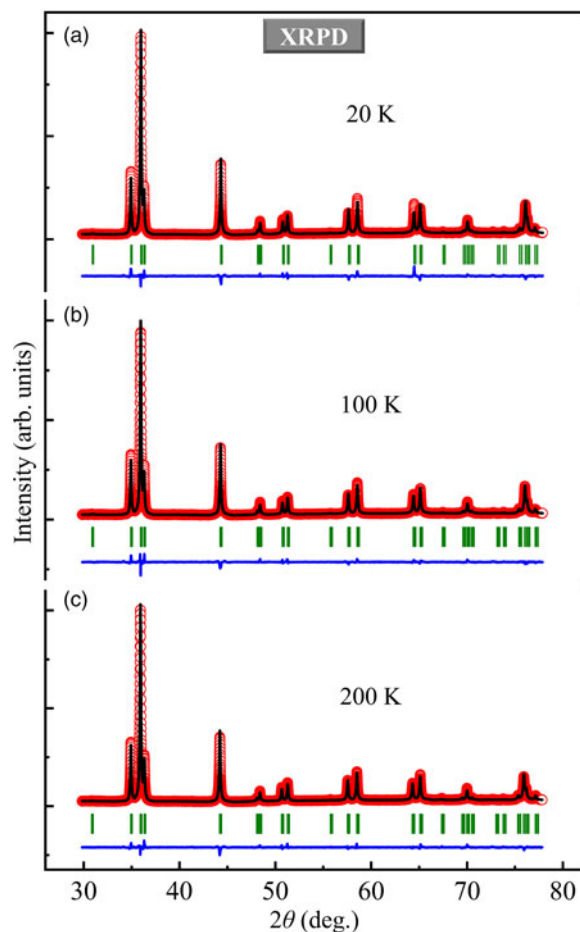
Figure 5. Observed (circles) and calculated (solid lines) in-house X-ray powder diffraction patterns of a pulverized $ErPd_2Si_2$ single crystal collected at (a) 20 K, (b) 100 K, and (c) 200 K. Vertical bars mark the positions of Bragg reflections. The bottom curves represent the difference between observed and calculated patterns. The diffraction angle 2θ range is from 30 to 78°.

TABLE IV. Extracted structural parameters of an intermetallic $ErPd_2Si_2$ single crystal from the XRPD study, including unit-cell parameters a and c, unit-cell volume V, calculated density D_{cal}, atomic positions, and isotropic thermal parameter (B), obtained from FULLPROF refinements of the XRPD data collected on an in-house X-ray diffractometer at 20, 100, and 200 K.

XRPD study of a pulverized $ErPd_2Si_2$ single crystal			
(Tetragonal, space group: *I4/mmm*)			
T (K)	20	100	200
a (Å)	4.08607(4)	4.08878(4)	4.09316(4)
c (Å)	9.89253(12)	9.88694(10)	9.88116(10)
V (Å³)	165.165(3)	165.291(3)	165.548(3)
D_{cal} (g cm⁻³)	8.772	8.765	8.752
Er	2a: (0, 0, 0)		
B (Er) (Å²)	2.01(4)	2.38(3)	2.35(3)
Pd	4d: (0, 0.5, 0.25)		
B (Pd) (Å²)	2.39(4)	2.75(3)	3.22(3)
Si	4e: (0, 0, z)		
z (Si)	0.37655(24)	0.37631(23)	0.37653(23)
B (Si) (Å²)	2.49(7)	3.97(7)	4.25(7)
R_p	3.35	3.08	2.96
R_{wp}	4.99	4.20	4.11
R_{exp}	3.45	3.51	3.49
χ^2	2.09	1.43	1.38

The numbers in parenthesis are the estimated standard deviations of the (next) last significant digit.

IV. CONCLUSION

$ErPd_2Si_2$ single crystals were grown using a laser-diode FZ furnace. We performed SXRPD and in-house XRPD studies from 20 to 500 K on a pulverized $ErPd_2Si_2$ single crystal. The FULLPROF refinements demonstrate that there is no structural phase transition in the studied temperature range, and the tetragonal *I4/mmm* space group is maintained. The refined unit-cell parameters display an elongation in the basal *ab* plane and a shrinkage along the *c*-axis, resulting in a larger unit-cell volume upon warming. This study provides temperature-dependent crystallographic information of single-crystal $ErPd_2Si_2$ compound, which would serve as an important basis for further experimental and theoretical studies.

V. DEPOSITED DATA

CIF and RAW data files were deposited with ICDD. You may request this data from ICDD at info@icdd.com.

CONFLICTS OF INTEREST

The authors have no conflicts of interest to declare.

Bażela, W., Leciejewicz, J., Szytuła, A., and Zygmunt, A. (**1991**). "Magnetism of DyPd₂Si₂ and ErPd₂Si₂," J. Magn. Magn. Mater. **96**(1), 114–120.

Bażela, W., Baran, S., Leciejewicz, J., Szytuła, A., and Ding, Y. (**1997**). "Magnetic structures of TbPd₂Si₂ and TbPd₂Ge₂—a redetermination," J. Phys.: Condens. Matter **9**(10), 2267–2273.

Cao, C. D., Klingeler, R., Leps, N., Vinzelberg, H., Kataev, V., Muranyi, F., Tristan, N., Teresiak, A., Zhou, S., Löser, W., Behr, G., and Büchner, B. (**2008**). "Interplay between kondo-like behavior and short-range antiferromagnetism in EuCu₂Si₂ single crystals," Phys. Rev. B **78**(6), 064409.

Cao, C. D., Klingeler, R., Leps, N., Behr, G., and Löser, W. (**2014**). "Single crystal growth of the ErPd₂Si₂ intermetallic compound," J. Cryst. Growth **401**, 601–604.

de Wolff, P. M. (**1968**). "A simplified criterion for the reliability of a powder pattern," J. Appl. Crystallogr. **1**, 108–113.

Frontzek, M. D. (**2009**). *Magnetic Properties of R₂PdSi₃ (R = Heavy Rare Earth) Compounds* (Cuvillier Verlag, Göttingen).

Li, H., Tian, W., Zarestky, J. L., Kreyssig, A., Ni, N., Bud'ko, S. L., Canfield, P. C., Goldman, A. I., McQueeney, R. J., and Vaknin, D. (**2009**).

"Magnetic and lattice coupling in single-crystal SrFe$_2$As$_2$: a neutron scattering study," Phys. Rev. B **80**(5), 054407.

Li, H.-F., Broholm, C., Vaknin, D., Fernandes, R. M., Abernathy, D. L., Stone, M. B., Pratt, D. K., Tian, W., Qiu, Y., Ni, N., Diallo, S. O., Zarestky, J. L., Bud'ko, S. L., Canfield, P. C., and McQueeney, R. J. (**2010**). "Anisotropic and quasipropagating spin excitations in superconducting Ba(Fe$_{0.926}$Co$_{0.074}$)$_2$As$_2$," Phys. Rev. B **82**, 140503(R).

Li, H.-F., Wildes, A., Hou, B., Zhang, C., Schmitz, B., Meuffels, P., Roth, G., and Bückel, T. (**2014**). "Magnetization, crystal structure and anisotropic thermal expansion of single-crystal SrEr$_2$O$_4$," RSC Adv. **4**(96), 53602–53607.

Li, H.-F., Cao, C., Wildes, A., Schmidt, W., Schmalzl, K., Hou, B., Regnault, L.-P., Zhang, C., Meuffels, P., Löser, W., and Roth, G. (**2015**). "Distinct itinerant spin-density waves and local-moment antiferromagnetism in an intermetallic ErPd$_2$Si$_2$ single crystal," Sci. Rep. **5**(1), 7968.

Li, H.-F., Zhu, Y. H., Wu, S., and Tang, Z. K. (**2021**). "A method of centimeter-sized single crystal growth of chromate compounds and related storage device," China Patent CN110904497B (China National Intellectual Property Administration, Beijing, China).

Mazilu, I., Teresiak, A., Werner, J., Behr, G., Cao, C. D., Löser, W., Eckert, J., and Schultz, L. (**2008**). "Phase diagram studies on Er$_2$PdSi$_3$ and ErPd$_2$Si$_2$ intermetallic compounds," J. Alloys Compd. **454**(1), 221–227.

Prokofiev, A. (**2018**). "Floating zone growth of intermetallic compounds," in *Crystal Growth of Intermetallics*, edited by P. Gille and Y. Grin (De Gruyter, Berlin, Boston), pp. 91–116.

Rodrĺguez-Carvajal, J. (**1993**). "Recent advances in magnetic structure determination by neutron powder diffraction," Phys. B: Condens. Matter **192**(1), 55–69.

Rotter, M., Tegel, M., and Johrendt, D. (**2008**). "Superconductivity at 38 K in the iron arsenide (Ba$_{1-x}$K$_x$)Fe$_2$As$_2$," Phys. Rev. Lett. **101**(10), 107006.

Sampathkumaran, E. V., Frank, K. H., Kalkowski, G., Kaindl, G., Domke, M., and Wortmann, G. (**1984**). "Valence instability in YbPd$_2$Si$_2$: magnetic susceptibility, X-ray absorption, and photoemission studies," Phys. Rev. B **29**(10), 5702–5707.

Sampathkumaran, E. V., Mohapatra, N., Iyer, K. K., Cao, C. D., Löser, W., and Behr, G. (**2008**). "Magnetic anomalies in single crystalline ErPd$_2$Si$_2$," J. Magn. Magn. Mater. **320**(8), 1549–1552.

Sasmal, K., Lv, B., Lorenz, B., Guloy, A. M., Chen, F., Xue, Y.-Y., and Chu, C.-W. (**2008**). "Superconducting Fe-based compounds ($A_{1−x}$Sr$_x$)Fe$_2$As$_2$ with A = K and Cs with transition temperatures up to 37 K," Phys. Rev. Lett. **101**(10), 107007.

Sefat, A. S., Jin, R., McGuire, M. A., Sales, B. C., Singh, D. J., and Mandrus, D. (**2008**). "Superconductivity at 22 K in Co-doped BaFe$_2$As$_2$ crystals," Phys. Rev. Lett. **101**(11), 117004.

Shatruk, M. (**2019**). "ThCr$_2$Si$_2$ structure type: the "perovskite" of intermetallics," J. Solid State Chem. **272**, 198–209.

Smith, G. S., and Snyder, R. L. (**1979**). "F$_N$: a criterion for rating powder diffraction pattern and evaluating the reliability of powder indexing," J. Appl. Crystallogr. **12**, 60–65.

Stewart, G. R. (**2001**). "Non-Fermi-liquid behavior in d- and f-electron metals," Rev. Mod. Phys. **73**(4), 797–855.

Szytuła, A., Jaworska-Gołab, T., Baran, S., Penc, B., Leciejewicz, J., Hofmann, M., and Zygmunt, A. (**2001**). "Magnetic structure of HoPd$_2$Si$_2$ redefined on the basis of new neutron diffraction data," J. Phys.: Condens. Matter **13**(35), 8007–8014.

Tang, C. C., Thompson, S. P., Hill, T. P., Wilkin, G. R., and Wagner, U. H. (**2015**). "Design of powder diffraction beamline (BL-I11) at diamond," in *Tenth European Powder Diffraction Conference: Geneva, September 1–4, 2006*, edited by Deutsche Gesellschaft für Kristallographie (Oldenbourg Wissenschaftsverlag, München), pp. 153–158.

Thompson, S. P., Parker, J. E., Potter, J., Hill, T. P., Birt, A., Cobb, T. M., Yuan, F., and Tang, C. C. (**2009**). "Beamline I11 at diamond: a new instrument for high resolution powder diffraction," Rev. Sci. Instrum. **80**(7), 075107.

Tomala, K., Sánchez, J., Malaman, B., Venturini, G., Blaise, A., Kmif, R., and Ressouche, E. (**1994**). "Magnetic properties of ErPd$_2$Si$_2$ from magnetization mössbauer and neutron diffraction measurements," J. Magn. Magn. Mater. **131**, 345–355.

Torikachvili, M. S., Bud'ko, S. L., Ni, N., and Canfield, P. C. (**2008**). "Pressure induced superconductivity in CaFe$_2$As$_2$," Phys. Rev. Lett. **101**(5), 057006.

Uchima, K., Uwatoko, Y., and Shigeoka, T. (**2018**). "Magnetic characteristics of RPd$_2$si$_2$ (R = Rare earth)," AIP Adv. **8**(10), 101425.

Wu, S., Zhu, Y., Gao, H., Xiao, Y., Xia, J., Zhou, P., Ouyang, D., Li, Z., Chen, Z., Tang, Z., and Li, H.-F. (**2020**). "Super-necking crystal growth and structural and magnetic properties of SrTb$_2$O$_4$ single crystals," ACS Omega **5**(27), 16584–16594.

Xu, Y.-K., Liu, L., Wolfgang, L., and Ge, B.-M. (**2011**). "Precipitates identification in R_2PdSi$_3$ (R = Pr, Tb and Gd) single crystal growth," Trans. Nonferrous Met. Soc. China **21**(11), 2421–2425.

Yakinthos, J. K., and Gamari-Seale, H. (**1982**). "Magnetic properties of some RPd$_2$Si$_2$ compounds (R = Gd, Tb, Dy, Ho and Er)," Eur. Phys. J. B **48**(3), 251–254.